Shallow Q_P and Q_S estimation from multicomponent VSP data

Michelle C. Montano, Don C. Lawton, and Gary F. Margrave

ABSTRACT

VSP data give us direct access to the wavelet at different receiver depths without having to include reflections. The down-going wavefield has always been the key to estimate Q and correct the effects of seismic attenuation on the data. In this study we demonstrate that we can also use the up-going wavefield to estimate Q, particularly for the shallow, near-surface layers. Q factors are estimated from synthetic VSP down-going and up-going wavefields by using the dominant frequency matching method (CREWES). We also estimated Q from real VSP data by using the spectral-ratio method (Vista software) as well as the dominant frequency matching method. We found the spectral-ratio method to be more sensitive to changes in the frequency bandwidth when we compare Q estimation from vibrator to dynamite sources. Also, we found that Q estimation for shallow layers is better using the up-going wavefield than the down-going wavefield. Combining both estimations provides the optimum understanding of Q variation with depth.

INTRODUCTION

Estimating Q on the shallow down-going wavefield has been always a difficult task because the receivers are close to the source and this causes an oversaturation in the amplitudes. Also, the wavefield has propagated for a short period of time and we may not see significant attenuation when we process our seismic data. However, shallow layers are expected to show low Q values because poorly consolidated rocks are usually present. One way to approach this problem is using the up-going wavefield to estimate Q in the shallow zone. By assuming that the source is at the reflecting interface, the receivers located in the shallow zone will be far from it.

THEORY

This study is based on the constant Q theory of Kjartansson (1979) which is a first order explanation of how the wavelet changes in an attenuating medium. This theory explains the wavelet decay in time and frequency. Also, there is an associated phase rotation. According to this, the amplitude spectrum of the wavelet after a traveltime, *t*, will be determined by the following equation:

$$W(f,t) = |W_0(f)|e^{-\frac{\pi f t}{Q}}, \tag{1}$$

where $|W_0(f)|$ is the initial amplitude spectrum, f is frequency and Q, the quality factor, is a rock property independent of frequency, although time dependence is allowed. Given the amplitude spectrum, the phase spectrum ($\Phi(w)$) is given by the Hilbert transform (Margrave, 2013):

$$\Phi(w) = H\big(ln(|W(f,t)|)\big). \tag{2}$$

Constant Q theory also predicts that velocity is frequency dependent and can be computed by the following equation (Aki and Richards, 2002):

$$V(f) = V_0\left[1 + \frac{1}{\pi Q} ln\left(\frac{f}{f0}\right)\right], \tag{3}$$

where f_0 is the reference frequency at which V_0 is specified and f is the frequency that we are interested in calculating the phase velocity.

Methods for Q estimation

Spectral-ratio

If we consider two wavelets at times t_1 and t_2, in which $t_1 < t_2$, their amplitude spectra will be the following:

$$|\hat{w}(t_1, f)| = |\hat{w}(f)|e^{-\frac{\pi f t_1}{Q}}. \quad (4)$$

$$|\hat{w}(t_2, f)| = |\hat{w}(f)|e^{-\frac{\pi f t_2}{Q}}. \quad (5)$$

Then, the log spectral-ratio or *lsr* is the ratio of equations 4 and 5 (Margrave, 2013),

$$lsr(Q, \Delta t, f) = ln\frac{|\hat{w}(t_2,f)|}{|\hat{w}(t_1,f)|} = -\frac{\pi f \Delta t}{Q}, \quad (6)$$

where $\Delta t = t_2 - t_1$. Equation 6 shows that *lsr* has a linear relationship with frequency. The interval Q between t_1 and t_2 can be computed by a least square fit of a first order polynomial. Note, however that noise and also notches can be a problem for the spectral division.

Dominant Frequency matching

Quan and Harris (1997) first introduced a frequency-shift method to estimate Q in which they defined the centroid frequency of the input signal $A_1(f)$ and the output signal $A_2(f)$ as

$$f_{C_1} = \frac{\int_0^\infty f A_1(f) df}{\int_0^\infty A_1(f) df}, \quad (7)$$

and,

$$f_{C_2} = \frac{\int_0^\infty f A_2(f) df}{\int_0^\infty A_2(f) df}. \quad (8)$$

In the discrete domain we can rewrite these equations as

$$fc_1 = \frac{\sum_{k=1}^n f(A_1)^2}{\sum_{k=1}^n (A_1)^2}. \quad (9)$$

$$fc_2 = \frac{\sum_{k=1}^n f(A_2)^2}{\sum_{k=1}^n (A_2)^2}, \quad (10)$$

where, $A_2 = A_1 T e^{-\frac{\pi f \Delta t}{Q}}$, T correspond to the frequency independent loss and Q represent the frequency-dependent attenuation. In the implementation of this method, a grid search over a range test values (*Qtest*) is performed until a minimum for the objective function in equation 11 is found.

$$Obj = (fc_1 - fc_2)^2 Qtest. \quad (11)$$

STUDY AREA

A walkaway vertical seismic profile was acquired in Alberta, which correspond to the well A (Figure 1). The location of the source points relative to the borehole is shown in Figure 2. These fourteen source points were acquired first with 0.125 kg of dynamite at 9 m depth, and then with an EnviroVibe source using a linear sweep of 10-300 Hz over 20 s (Hall et al., 2012). The near offset is at 12 m (shot point 1) and the far offset is at 1031 m (shot point 14).

The closest well log data available is from well B, located 200 meters north of the VSP (Figure 3). Well C and D are located approximately 500 meters of the VSP and also contain well log data. The well log data from well B were blocked into five constant horizontal layers by computing the average or mean value between the formation tops. Q values were computed using *fakeQ* from the CREWES toolbox. These values were used to perform forward modelling and to compute a synthetic VSP.

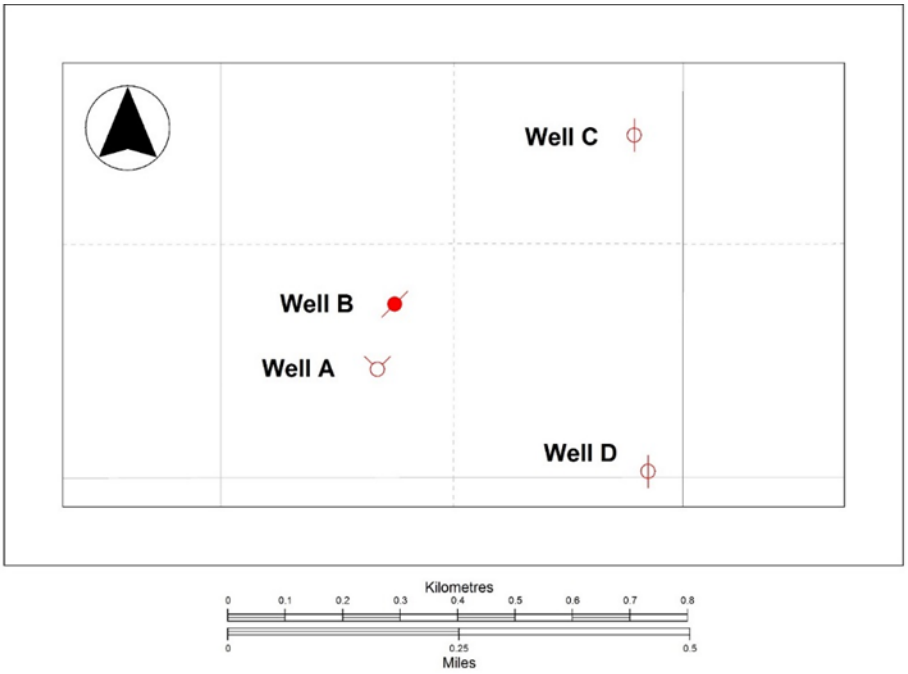

FIG. 1. Base map. VSP data from Well A and well log data from Well B were used in this study.

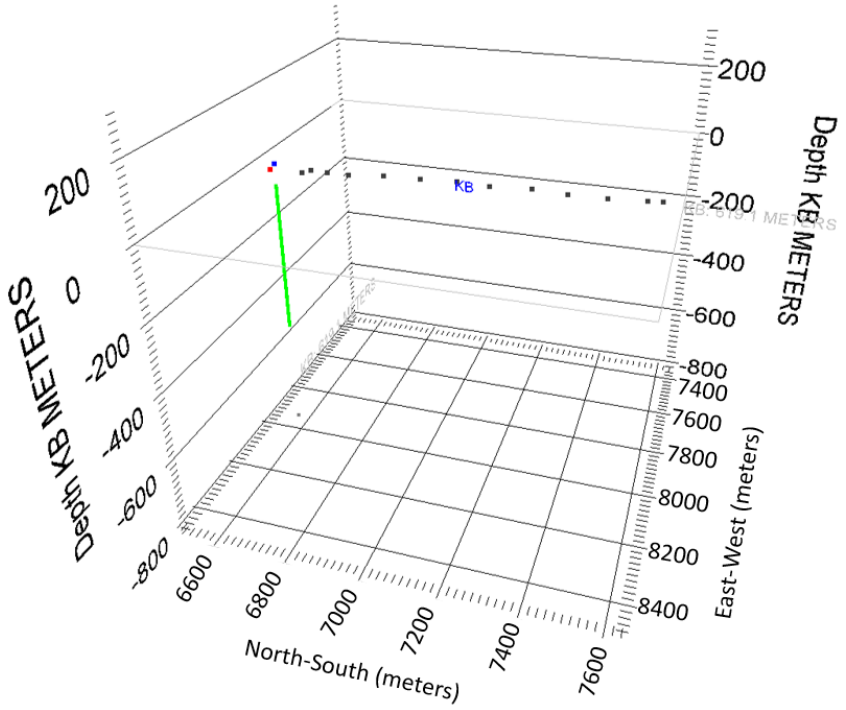

FIG. 2. VSP geometry using Vista software.

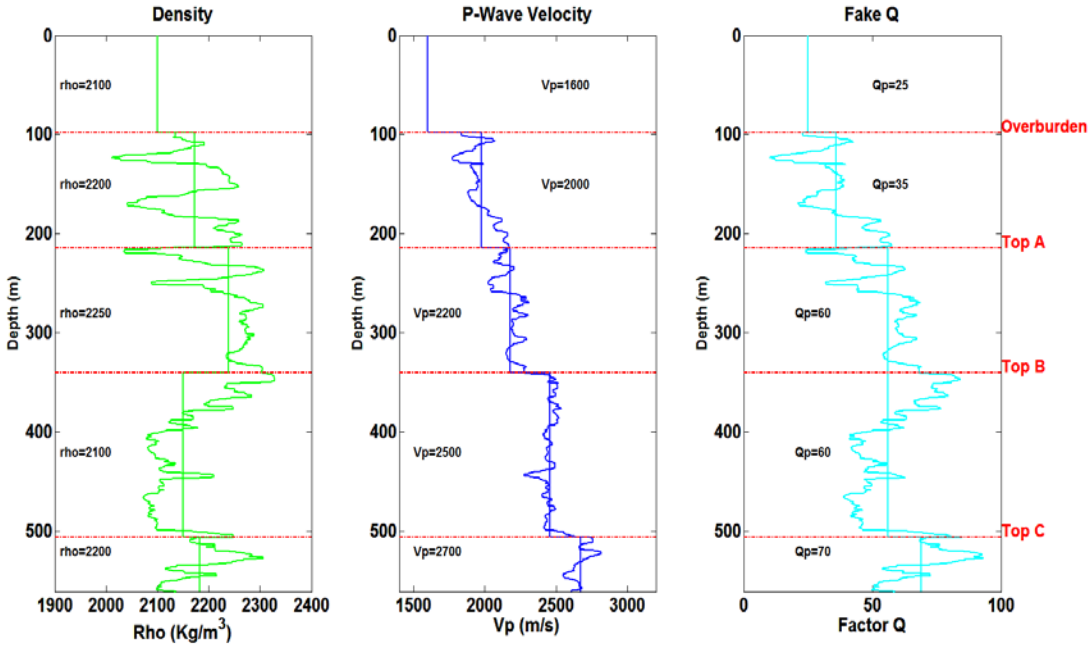

FIG. 3. Density and p-wave velocity log from Well B, blocked into five horizontal layers.

SYNTHETIC VSP DATA ANALYSIS

A 1D synthetic VSP was computed with *vspmodelq* from the CREWES toolbox (Figure 5). The forward modelling was performed using the blocked well log data from Well B which includes density, p-wave velocity and Q values computed with *fakeQ* (Figure 3). The zero offset source is at $z = 0$ and the receivers are located every 10 m from the initial depth, $z_i = 10\ m$ to the final depth, $z_f = 600\ m$. A minimum phase wavelet with a dominant frequency, $F_{dom} = 30\ Hz$ was also used for this computation.

Downgoing wavefield

Down-going waves propagate to the borehole receivers as shown in Figure 4. These first arrivals give us access to the wavelet at different depths without having to be concerned about reflections (Hinds et al., 1997). For this reason, most Q estimations are generally computed from the down-going wavefield. Figure 4 also shows that the source is closer to the shallow receivers. It may cause problems to estimate Q in the shallow layers because the wavefield has propagated a short period of time and we may not observe significant attenuation when we process our data.

Q_P values were estimated from the synthetic down-going wavefield using the dominant frequency method from the CREWES toolbox. For doing this, we created a receiver vector, Z_0, that contains the traces every 30 m (orange receivers, Figure 5). This vector was compared to a deeper vector, $Z_R = Z_0 + d$, where d is the distance from each receiver. For this case, we used different distances, d =30m, 50 m and 80 m. Figure 6 shows how the Q values were estimated for $d = 30$ m, where $Z_0 = (70{:}\,30{:}\,570)$ and $Z_R = (100{:}\,30{:}\,600)$. For example, if we estimate Q comparing two traces at 70 m and 100 m depth, the Q value corresponds to the receiver depth located between them, which is 85 m depth. Figure 7 shows the obtained Q values, where Q_{ins} corresponds to the instantaneous Q obtained from well log data, $Q_{estimation}$ corresponds to the values estimated from the synthetic down-going wavefield and Q_{ave} corresponds to the average Q given by equation 12, where $Q_k = Q_{ins}$,

$$Q_{ave}^{-1} = \frac{1}{t}\sum_{k=1}^{n}\frac{\Delta t_k}{Q_k}. \qquad (12)$$

For $d = 30\ m$ (Figure 7A), Q values estimated from 200-500 m depth do not show a good match with the average Q, and some of them are higher than the actual Q = 60. For $d = 50\ m$ (Figure 7B), we observed a better match between the average Q and the estimated Q along the borehole. For $d = 80\ m$ (Figure 7C), the estimated Q and the average Q has a good match from 200-500 m depth. However, for the interval between 50-200 m the average Q and the estimated Q differs from the instantaneous Q, particularly when they are close to the interface. Q values were also estimated by comparing a fixed trace at 220 m depth, $Z_0 = 220$, with a group of traces from 240-480 m depth, $Z_R = 240{:}\,30{:}\,480$ (Figure 7D). For this case, we observe a very good match because we are comparing traces in the same layer. Once we increase the length of the receiver vector from 240-600 m depth, $Z_R = 240{:}\,30{:}\,600$ (Figure 7E), the average Q and the estimated Q start to differ from the instantaneous Q because we are comparing traces from different layers with different Q values. Therefore, the optimun Q values estimated along the borehole were obtained with $d = 50\ m$. This result lead us to conclude that if we estimate Q from traces that are too close together, we may not obtain a good result due to the short interval of time that the wavefield has propagated, leading us to overestimate the actual Q values. On the other hand, Q estimation from traces that are too far, may cause errors because we have a higher risk because traces are from different layers.

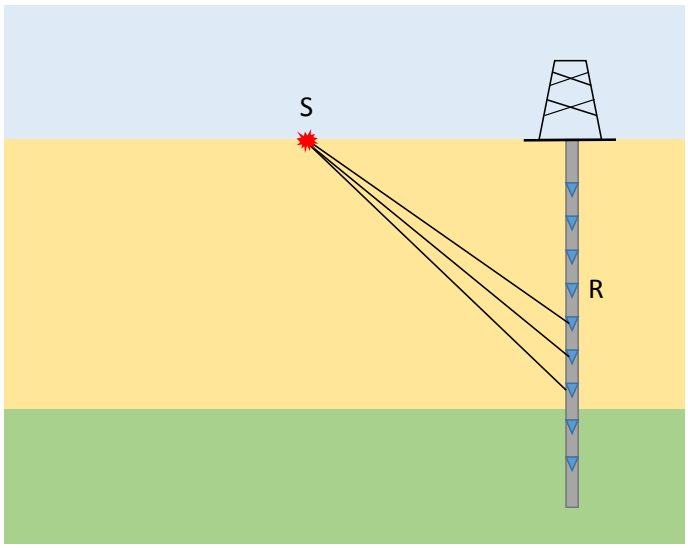

FIG. 4. Down-going waves propagating to the borehole receivers.

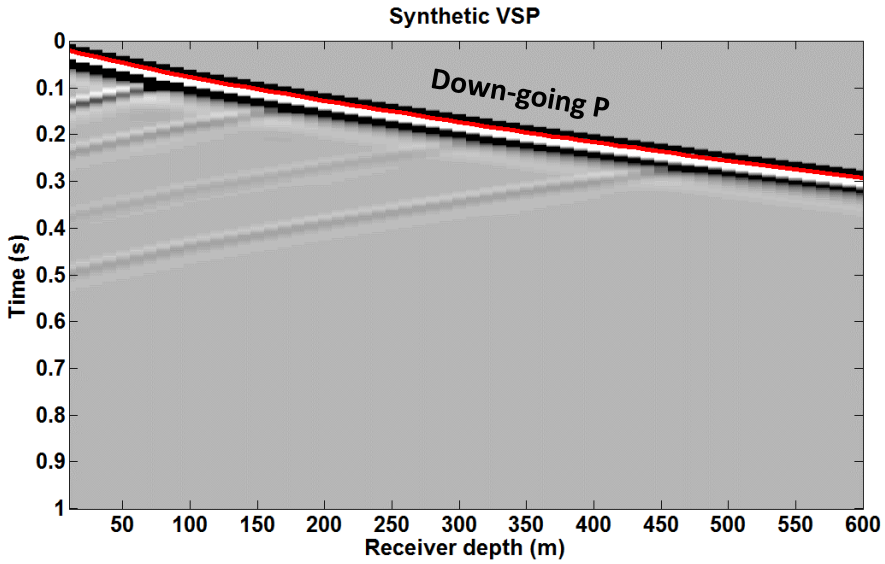

FIG. 5. Forward Modelling using well log data from Well B. Red line shows first breaks.

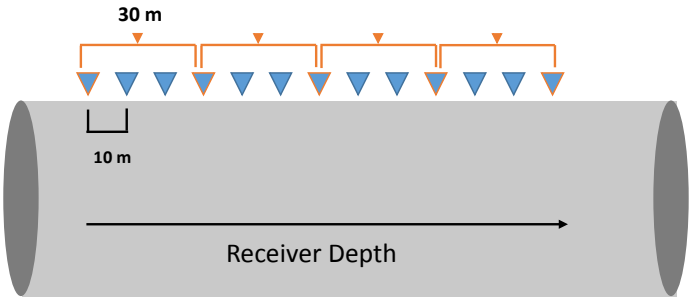

FIG. 6. Diagram for Q_P estimation from synthetic down-going wavefield using CREWES toolbox.

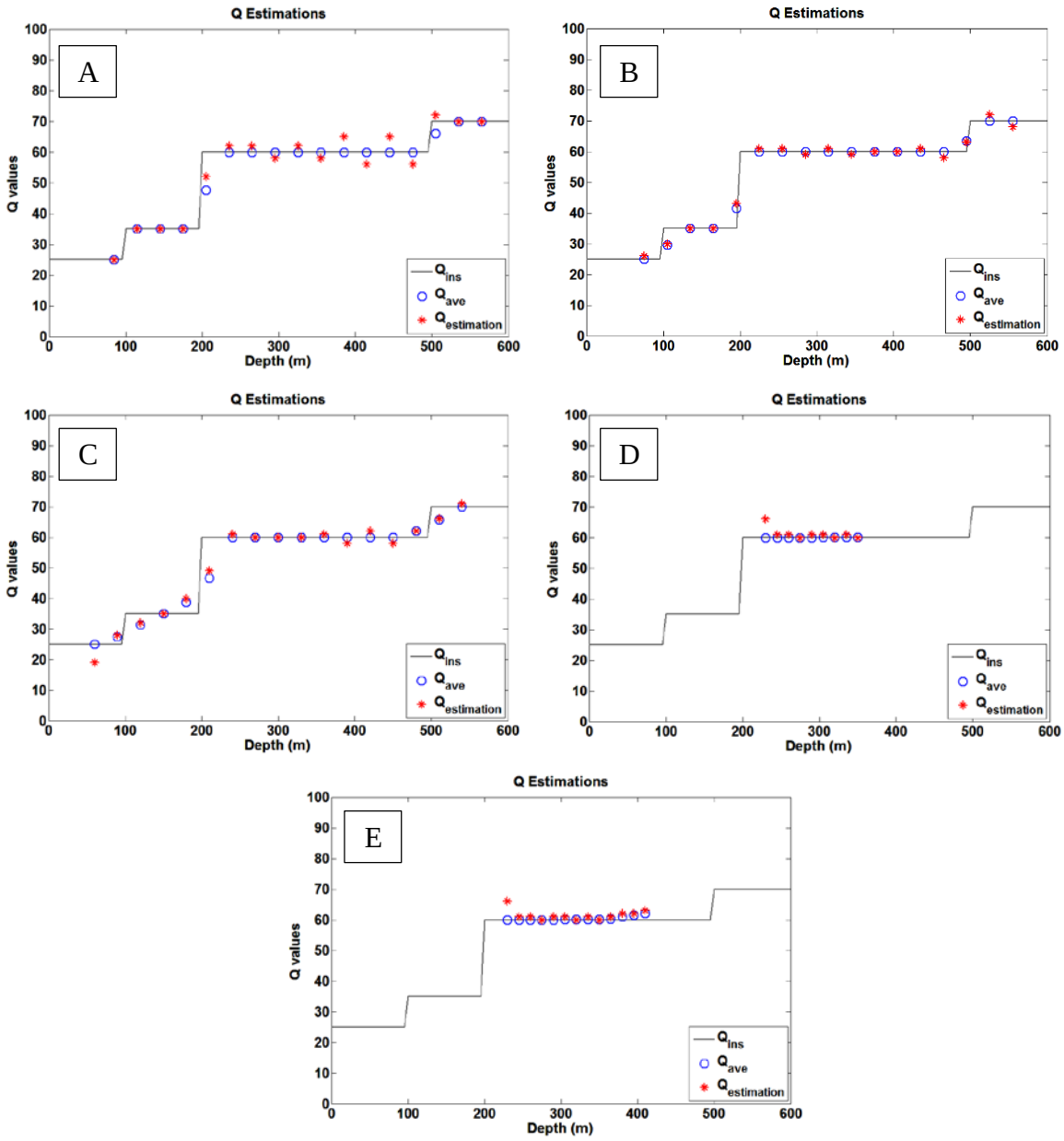

FIG. 7. Q_P estimation from down-going wavefield using dominant frequency method. A) For $d = 30\ m$, B) $d = 50\ m$, C) $d = 80\ m$, D) For a fixed traced, $Z_0 = 220$, and $Z_R = (240{:}\ 30{:}\ 480)$ and E) $Z_0 = 220$ and $Z_R = (240{:}\ 30{:}\ 600)$.

Upgoing wavefield

Q_P values were also estimated from the synthetic up-going wavefield. Figure 8 shows the up-going waves propagating to the borehole receivers, where S indicates the source and S* represents a secondary source located at the interface according to the Huygen's principle. As one can observe, this secondary source is closer to the deepest receivers and farther from the shallow receivers. It may help us to obtain a more accurate Q estimation in the shallow layer. For the Q analysis, we compared the traces after reflection, then we do not have to be concerned about transmission loss.

For this case, we chose the highest amplitude up-going event which is shown in Figure 9 (green line). The up-going wavefield was flipped to process this data as a down-going wavefield (Figure 10) but now comparing deeper traces with shallower traces.

Figure 11 shows the Q_P values obtained from this estimation. Notice that these estimated Q values have been flipped back to their real depth. For $d = 30\ m$ (Figure 11A), we also observed that the estimated Q do not show a good match with instantaneous Q in the third layer, where $Q = 60$. For $d = 50\ m$ (Figure 11B), the estimated Q match with the average Q along the borehole. For $d = 80\ m$ (Figure 11C), the estimated Q differs from the instantaneous Q, particularly when they are close to the interfaces. Then, we also estimated Q comparing a fixed trace at 480 m depth, $Z_0 = 480$, with a group of traces from 460-200 m depth, $Z_R = (460{:}\ 30{:}\ 200)$ (Figure 11D). In this case we also obtained a good result because all the traces are in the same layer, $Q = 60$. Once, we increased the length of the receiver vector from 460-0 m depth, we started to find some differences between the average Q and the instantaneous Q because we are including traces from different layers. For this case, the error is larger than the one obtained from the down-going wavefield because now we are changing from $Q = 35$ to $Q = 60$ (Figure 11E).

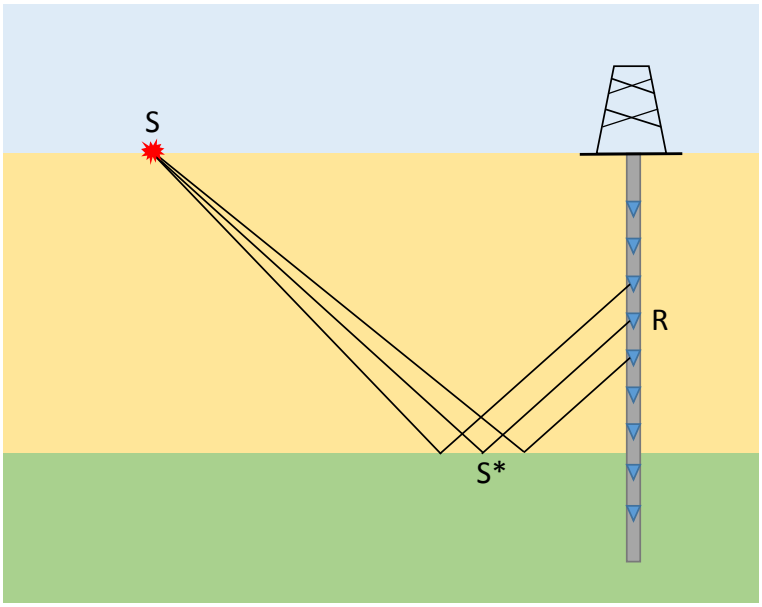

FIG. 8. Up-going waves propagating to the borehole receivers.

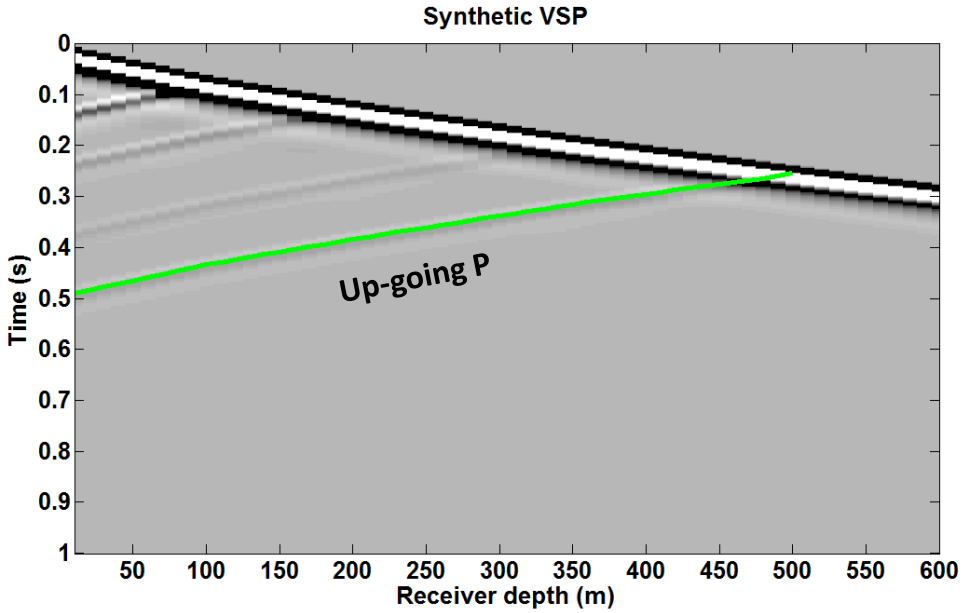

FIG. 9. Forward Modelling based on Well B, showing up-going events.

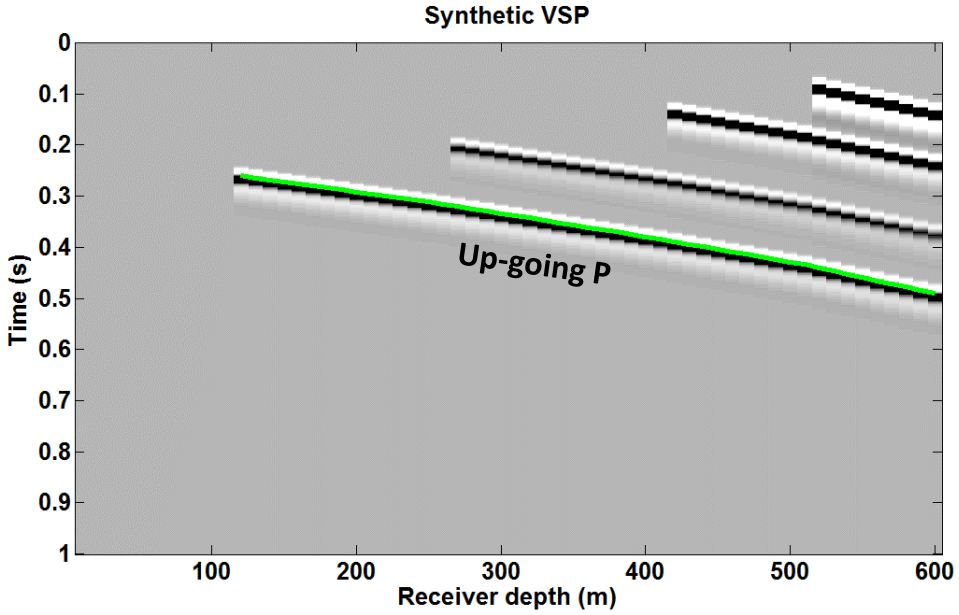

FIG. 10. Flipped up-going events in Figure 7. Notice that the reference event now shows the moveout of a down-going wavefield.

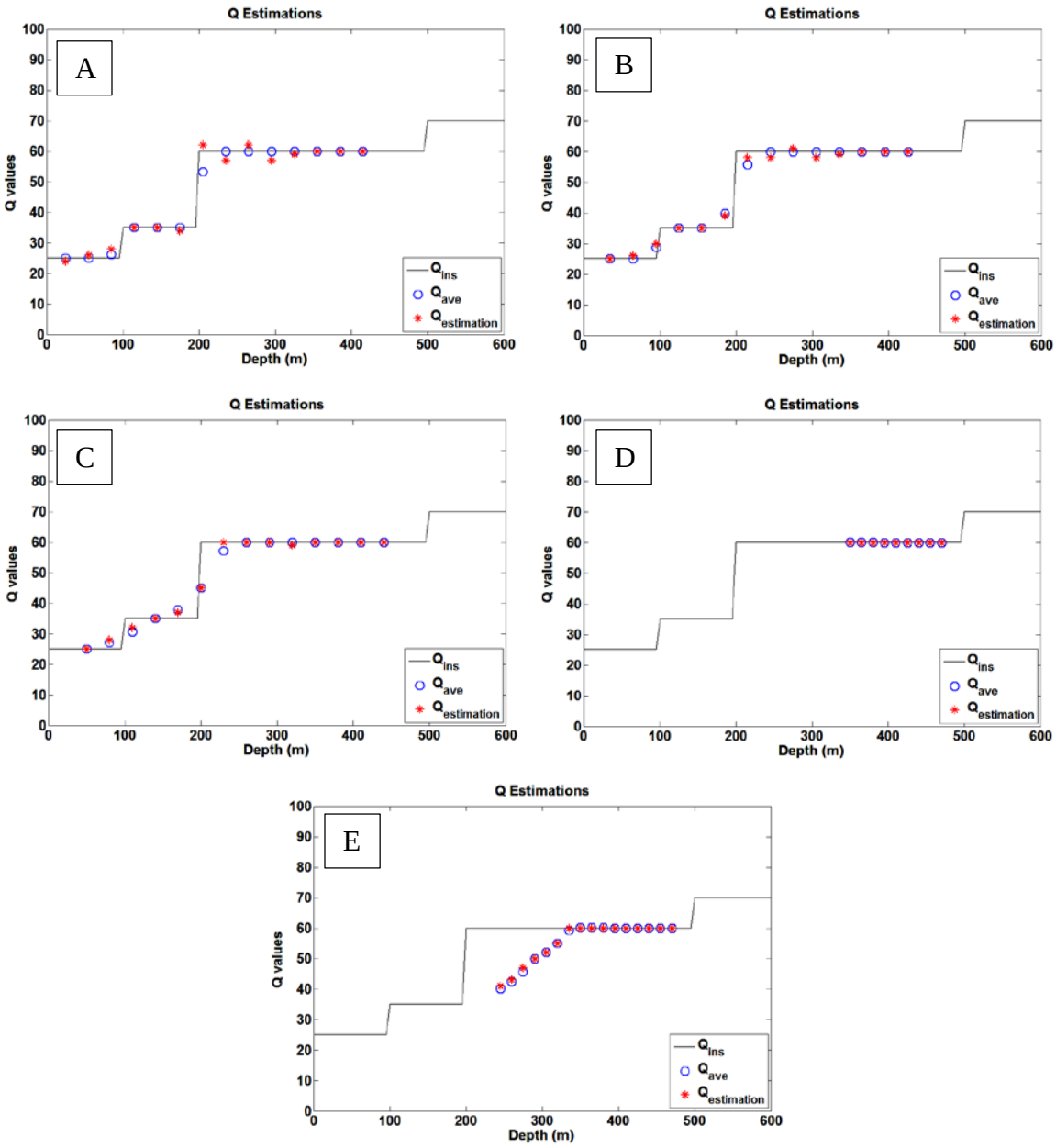

FIG. 11. Q_P estimation from the synthetic up-going wavefield using dominant frequency method. A) For $d = 30\ m$, B) $d = 50\ m$, C) $d = 80\ m$, D) For a fixed trace at 480 m depth, $Z_0 = 480$ and $Z_R = (460{:}\,30{:}\,200)$ and E) $Z_0 = 480, Z_R = (460{:}\,30{:}\,0)$.

FIELD VSP DATA ANALYSIS

Dynamite Source

Down-going wavefield analysis

Fourteen source points were acquired with 0.125 kg of dynamite at 9 m depth (Figure 2). Figure 12 shows the seismic gather of the shot point 1 which is at the nearest offset (12 m). The green line represents the first breaks. The amplitude spectra for the down-going wavefield was computed to choose the frequency window in the Q analysis (Figure 13). Before doing the Q analysis, we prepared the data using the flow in Table 1. We first input the geometry and picked the first breaks, then we flattened the first arrival at 100 ms and applied a median filter to separate the wavefield.

The Q_P values estimated from the down-going wavefield using spectral-ratio method in Vista software are shown in Figure 14. We obtained a higher Q value for the shallow layer, $Q = 138$, from 100-200 m depth. Then, these values gradually increase from $Q = 51$ to $Q = 62$ (Figure 14). This higher Q value in the shallow layer may be due to the short distance between the source and the top receivers, and we suspect this values to erroneous.

Table 1. Processing flow for Q estimation

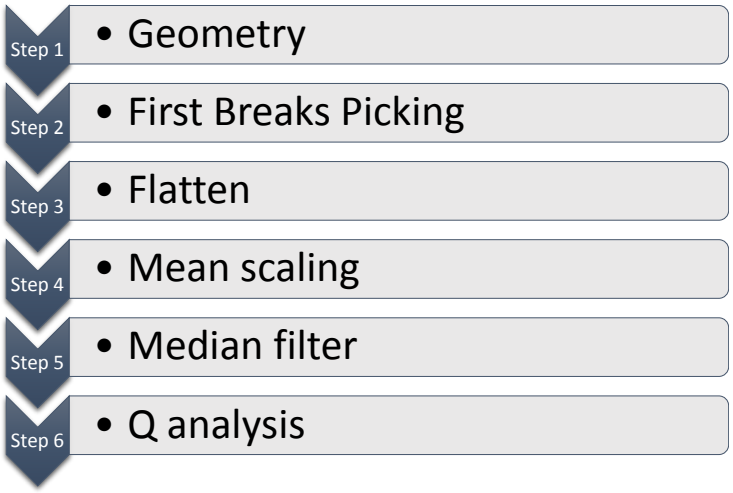

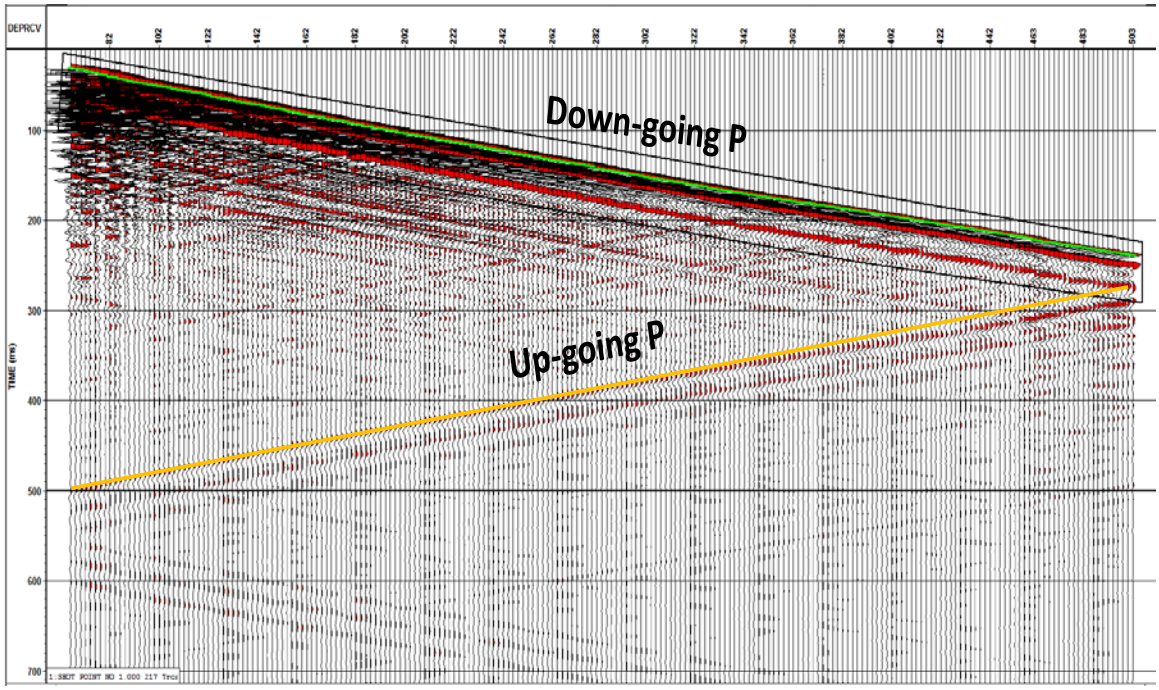

FIG. 12. Seismic gather for shot point 1 with a dynamite source (Z component). Green line shows the first breaks.

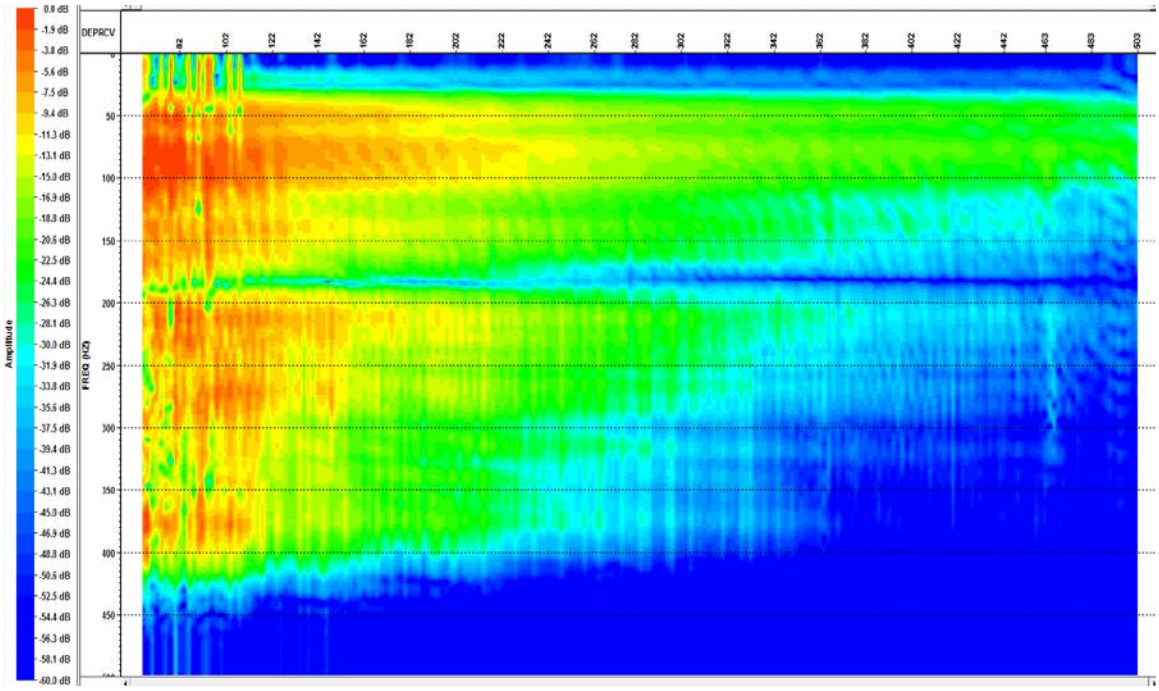

FIG. 13. Amplitude spectra of the down-going wavefield for shot point 1. Notice the shortening of band-width with increasing depth.

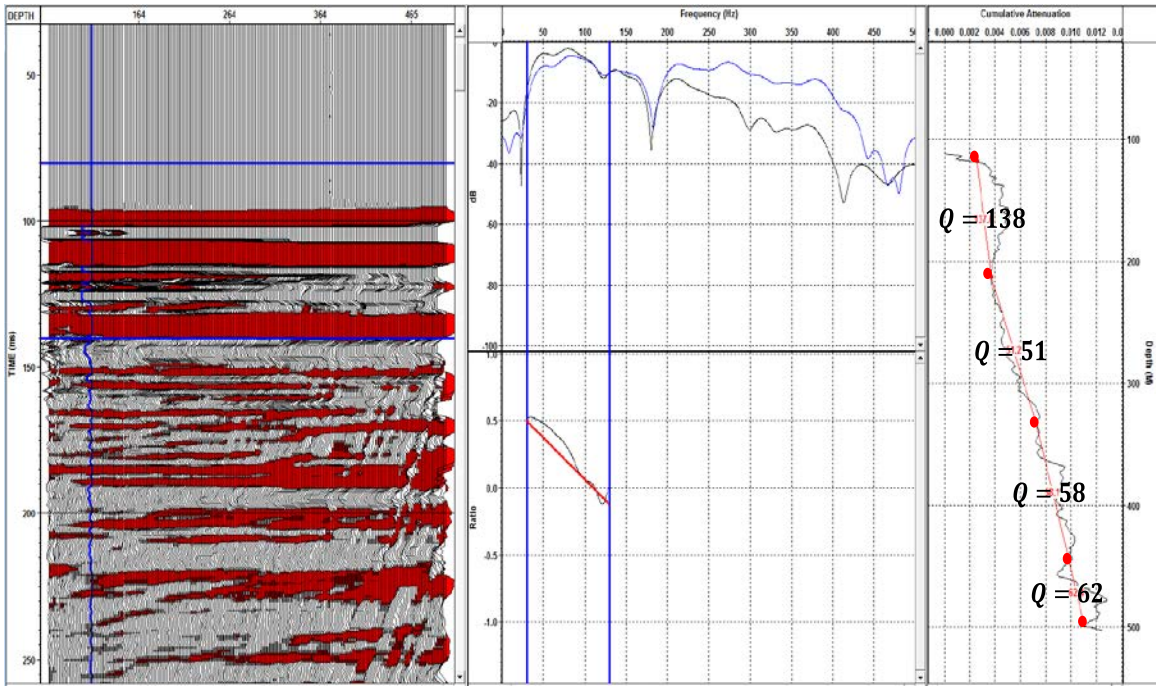

FIG. 14. Q_P estimation from down-going wavefield using spectral-ratio method (Vista software).

Up-going wavefield analysis

Q_P values were then estimated from the up-going wavefield using the spectral-ratio method in Vista software. The seismic data from shot point 1 was flipped to process the up-going wavefield as a down-going wavefield (Figure 15). Equation 13 was used to flip the receiver depth in the headers. Notice that the distance between receivers will be the same but now the top trace is the base one.

$$RD_{flipped} = shift - RD, \tag{13}$$

where RD is the receiver depth, $RD_{flipped}$ is the flipped receiver depth, and $shift$ is the maximum plus minimum receiver depth (566 m).

In the Figure 16, we observe the amplitude spectra of the up-going wavefield enclosed in the black box in Figure 15. Here, the frequency band expands from 30 to 100 Hz approximately. Q_P analysis is shown in Figure 17 in which the receiver depths are flipped and the deepest layer corresponds to the shallowest layer. For example, if we substitute a flipped receiver depth, $RD_{flipped} = 500\ m$ into the equation 13, we obtain the actual receiver depth, $RD = 66\ m$. The shallow interval from 66 to 146 m depth, the Q value estimated is, $Q = 20$. The interval from 146 to 266 m depth, $Q = 28$. From 266-346 m depth, $Q = 70$ and from 346-466 m depth, $Q = 187$.

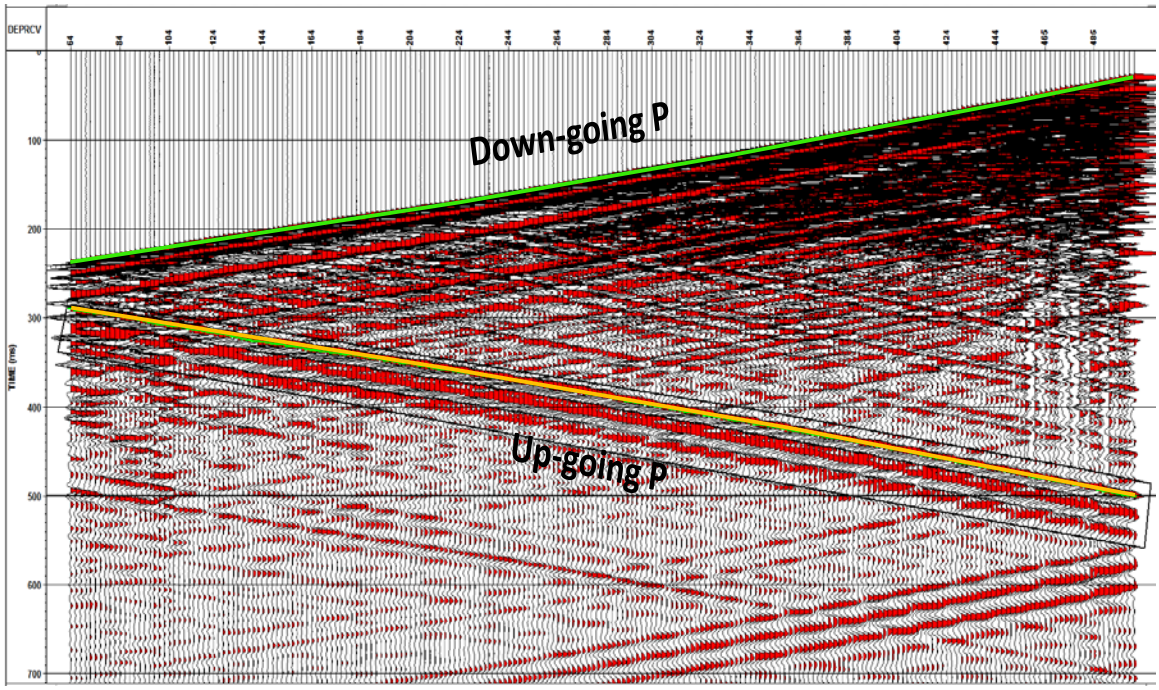

FIG. 15. Seismic gather for shot point 1 (flipped). The green line shows the up-going event.

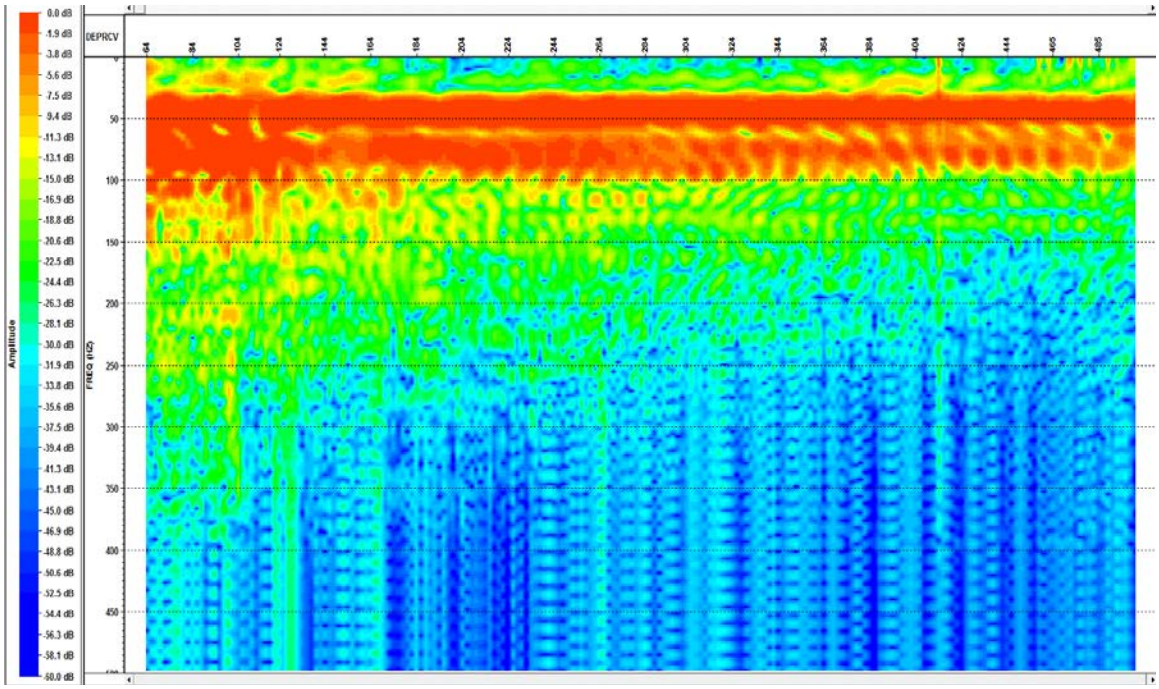

FIG. 16. Amplitude spectra of the up-going wavefield (flipped). Notice the loss of frequency bandwidth with increasing pseudo depth.

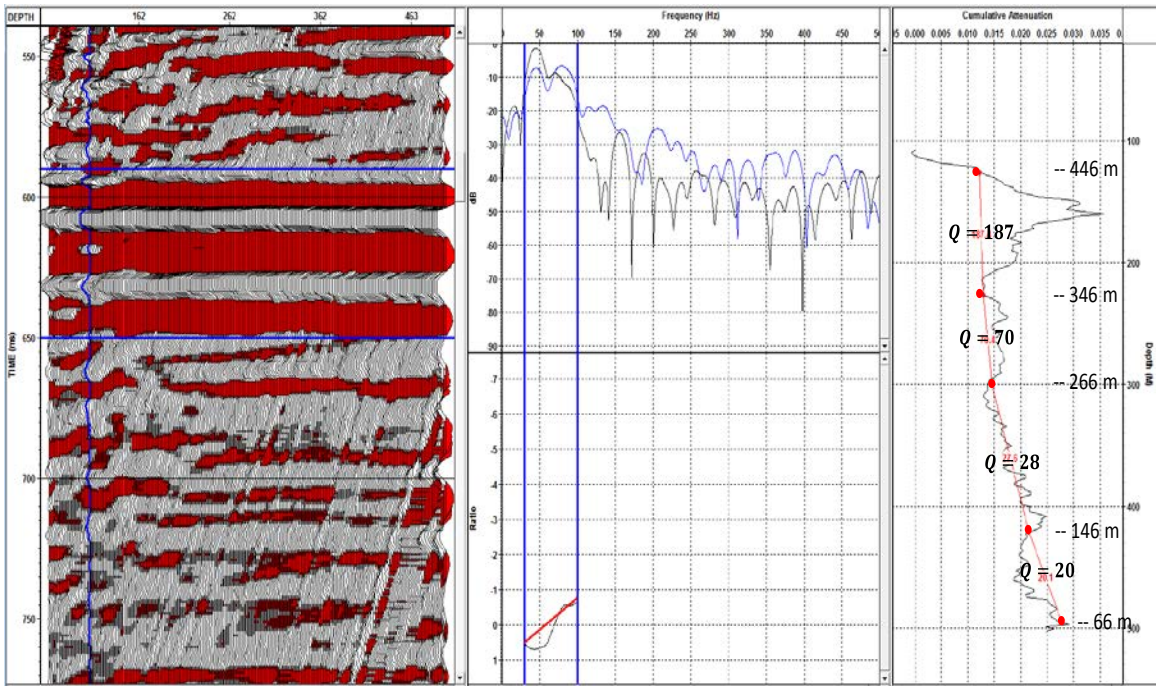

FIG. 17. Q_P estimation from up-going wavefield using spectral-ratio method (Vista software). Notice that receiver depths are flipped.

EnviroVibe source

Down-going wavefield analysis

The fourteen source points were also acquired with an EnviroVibe source with a linear sweep from 10-300 Hz over 20 s. In Figure 18 we observe the seismic gather of shot point 1. For this case, we only estimated Q from the down-going wavefield because the tube waves interfere with the up-going wavefield and there is more noise.

Figure 20 and 21 show the Q analysis using a frequency window of 30-250 Hz and 30-130 Hz, respectively. When we use a frequency window of 30-250 Hz (Figure 20), we observed that the Q values estimated are lower than the obtained from the down-going wavefield with a dynamite source (Figure 14). However, when we use the same frequency window from 30-130 Hz, we obtained similar Q values (Figure 21).

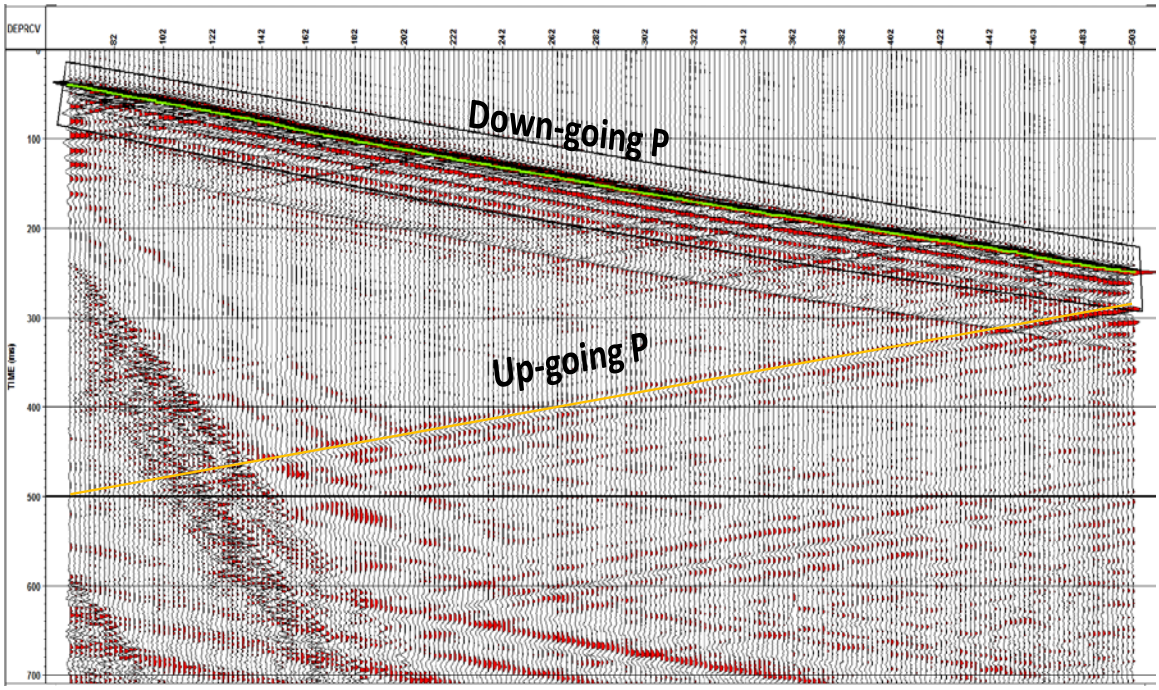

FIG. 18. Seismic gather for shot point 1 with an EnviroVibe source (Z component). The green line shows the first breaks.

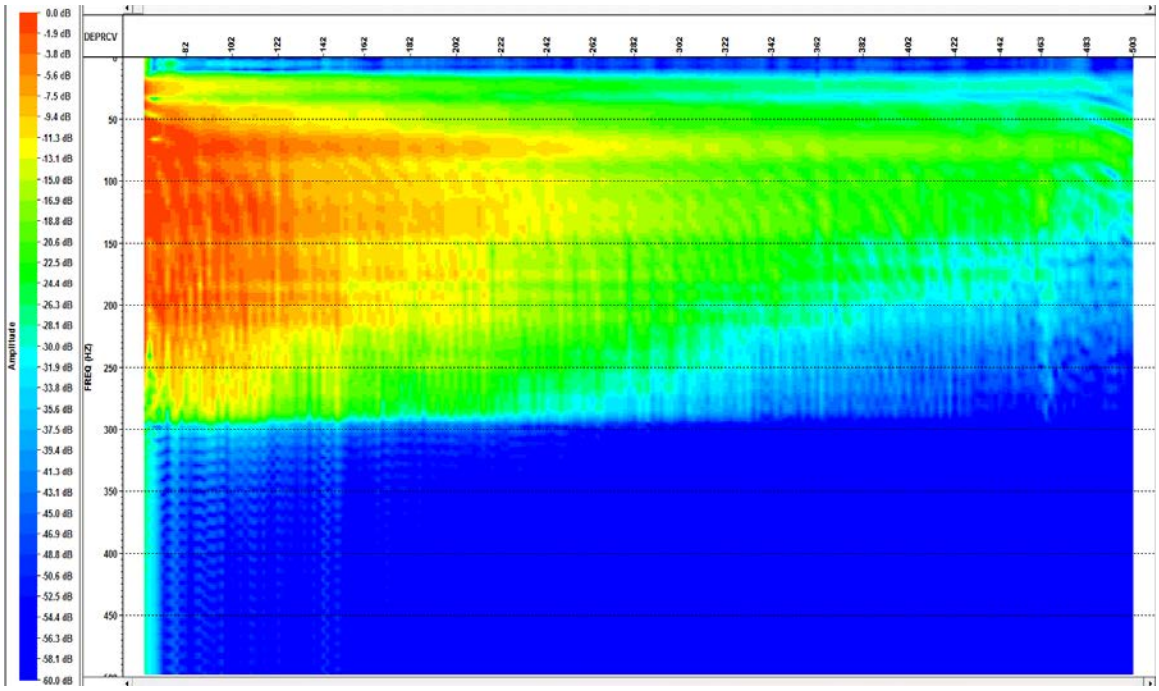

FIG. 19. Amplitude spectra of the down-going wavefield with an EnviroVibe source.

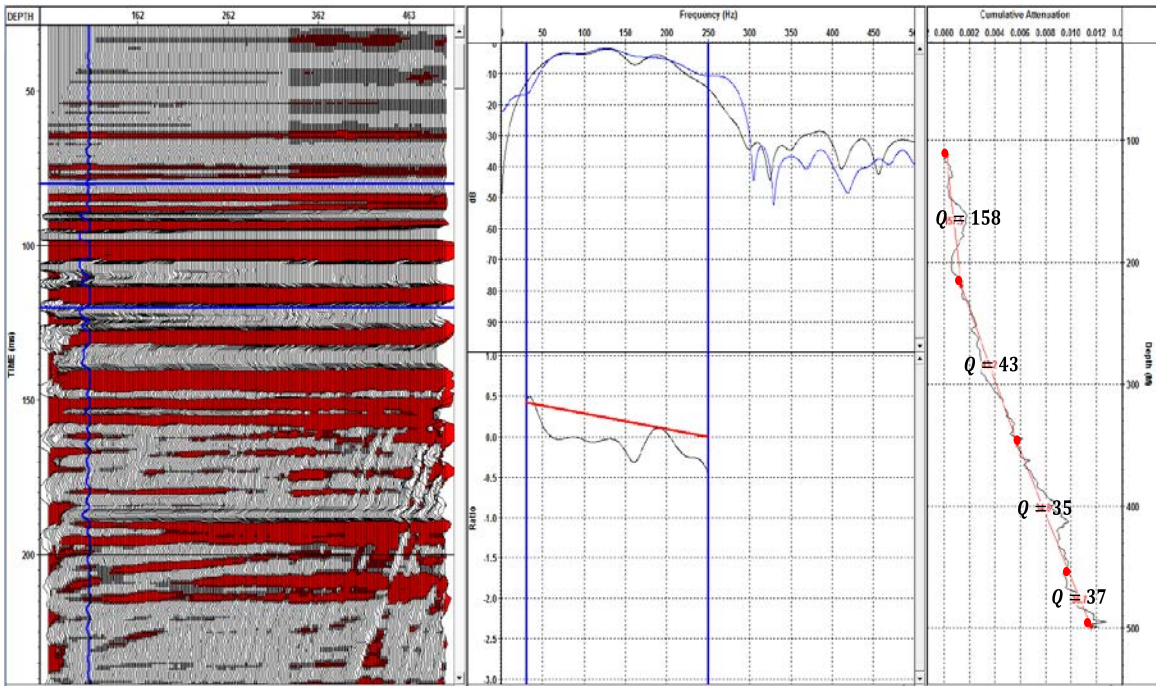

FIG. 20. Q_P estimation from down-going wavefield using spectral-ratio method (Vista software). Frequency window from 30 – 250 Hz.

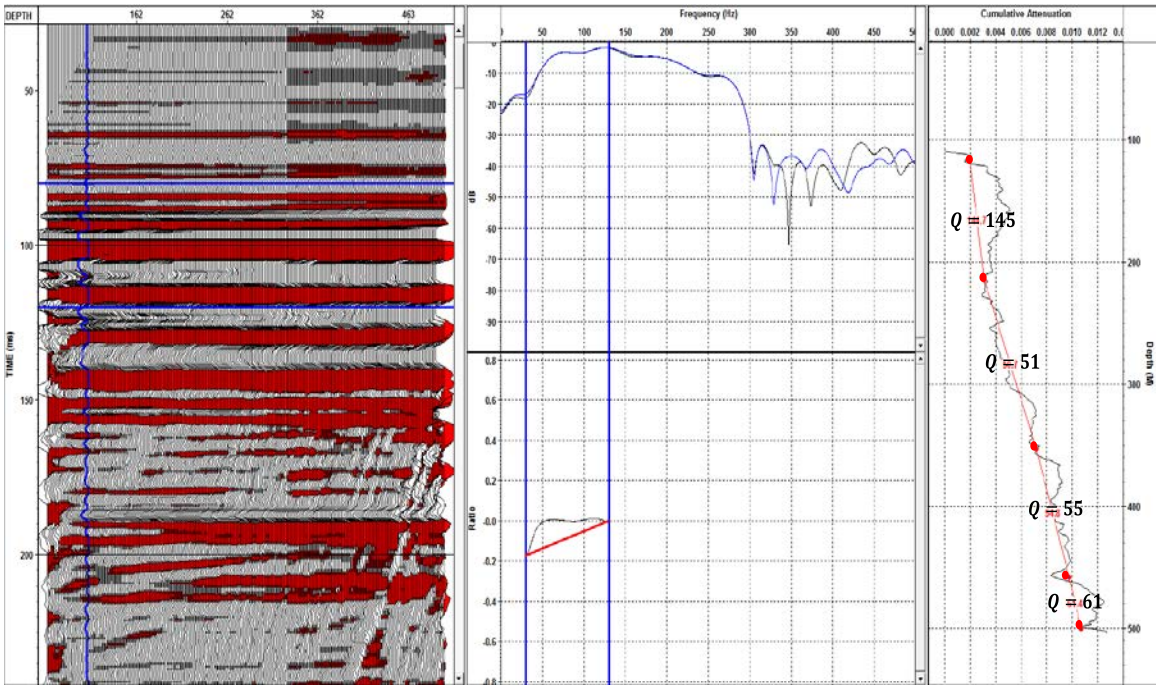

FIG. 21. Q_P estimation from down-going wavefield using spectral-ratio method (Vista software). Frequency window from 30 – 130 Hz.

Q_S Estimation from down-going wavefield

Figures 22 and 23 show the X and Y component of the shot point 1 with a EnviroVibe source. Here we can observed a direct down-going shear wavefield whose velocities range from 500-700 m/s. Most of the down-going wavefield is focussed on the X component but we also observed some energy in the Y component. For that reason, we rotated X and Y components to orientate the horizontal components toward the source (Hmax and Hmin) using hodogram analysis of the first arrivals. This results are shown in Figures 24 and 25. As one can see, we obtained similar result after rotation with some improvements in the continuity of the events in the Hmax gather (yellow box, Figure 24). The remaining energy in the Hmin gather may be due to the presence of anisotropy.

Q_S values were estimated from Hmax (Figure 22) which amplitude spectra is shown in Figure 26. We observed that the frequency ranges between 10-100 Hz and there is notch at 50 Hz. For the Q analysis, we chose a frequency window from 10-40 Hz to avoid this notch (Figure 27). The results obtained are: $Q_S = 100$ from 100 – 200 m depth, $Q_S = 21$ from 200 – 350 m depth, $Q_S = 34$ from 350 – 420 m depth, and $Q_S = 10$ from 420 – 500 m depth. These Q_S values are lower than the Q_P values obtained before (Figures 20 and 21).

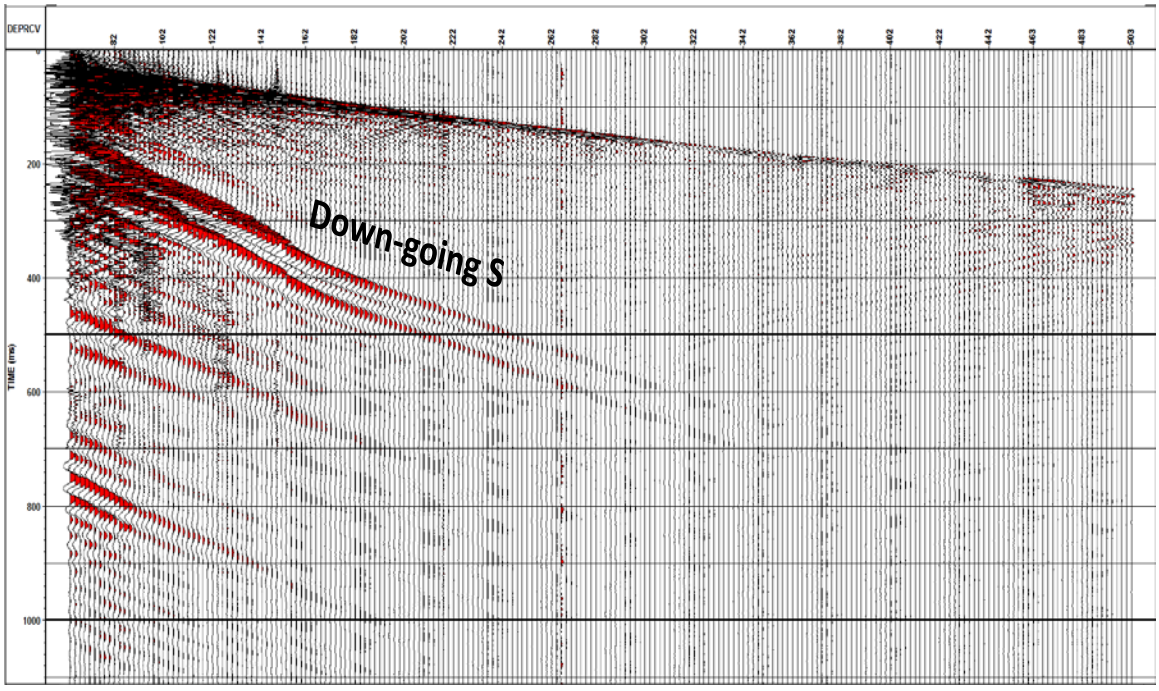

FIG. 22. Seismic gather for shot point 1 (X component).

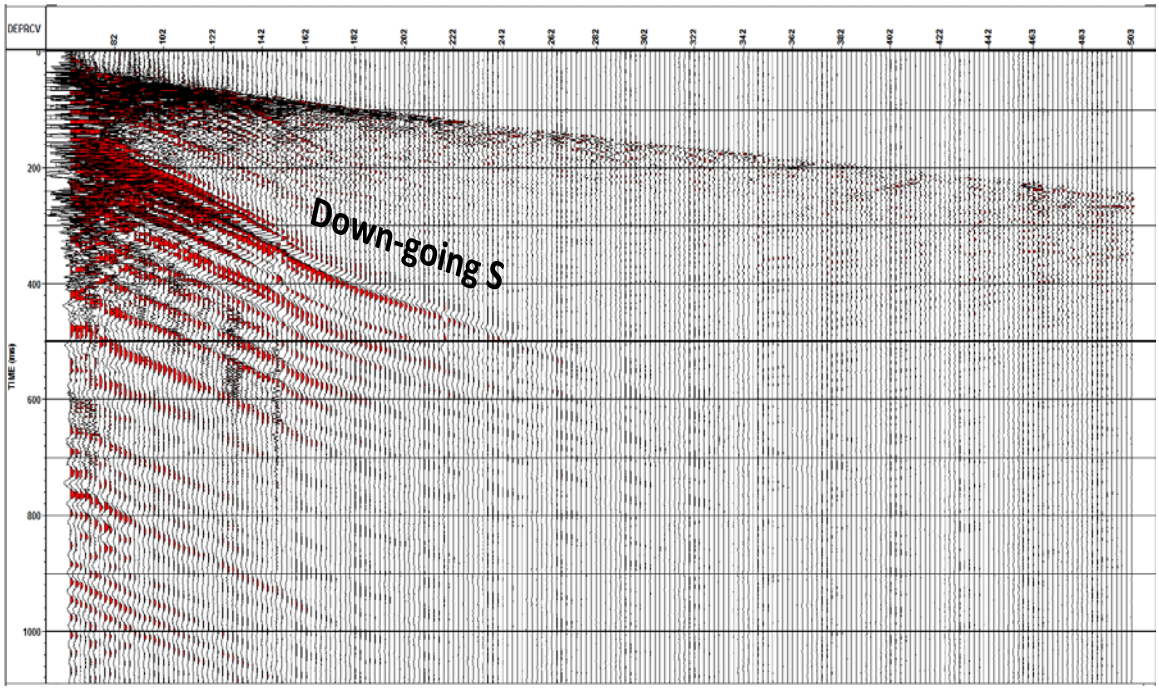

FIG. 23. Seismic gather for shot point 1 (Y component).

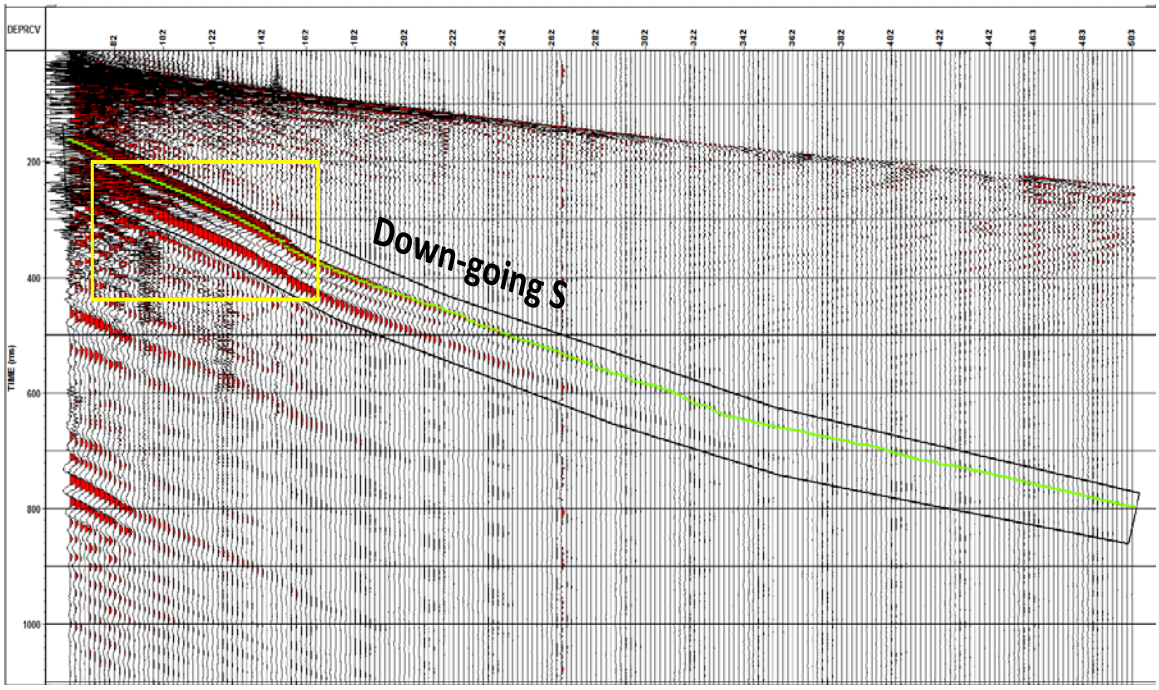

FIG. 24. Seismic gather for shot point 1 (X component – Hmax).

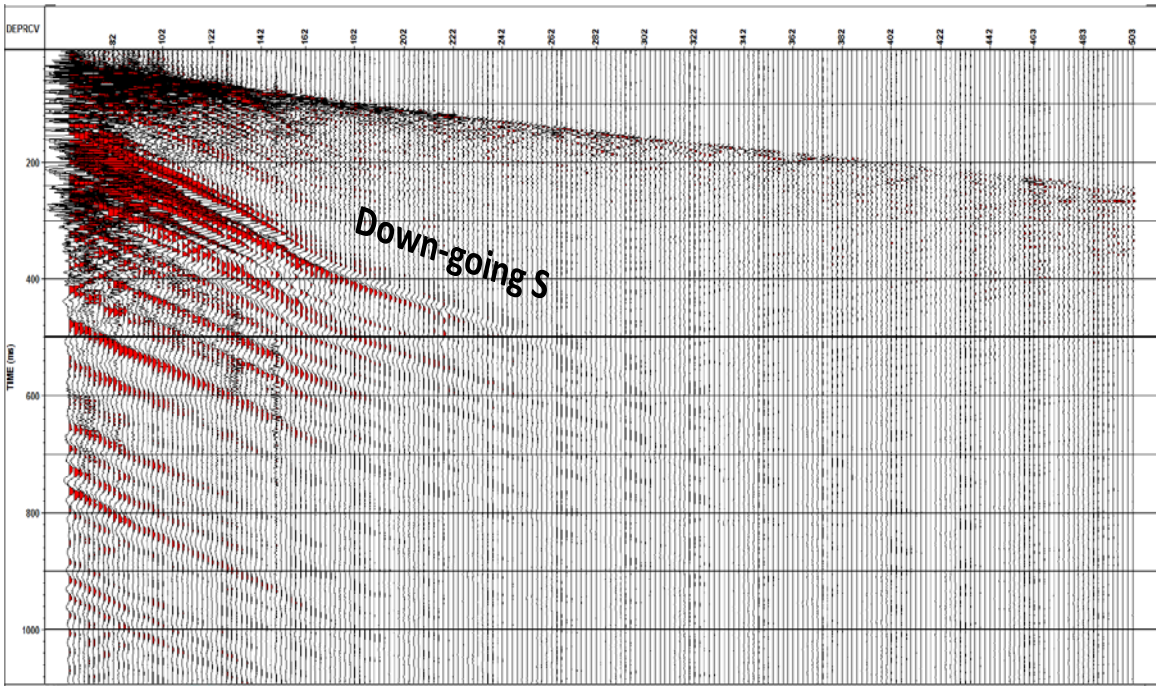

FIG. 25. Seismic gather for shot point 1 (Y component – Hmin).

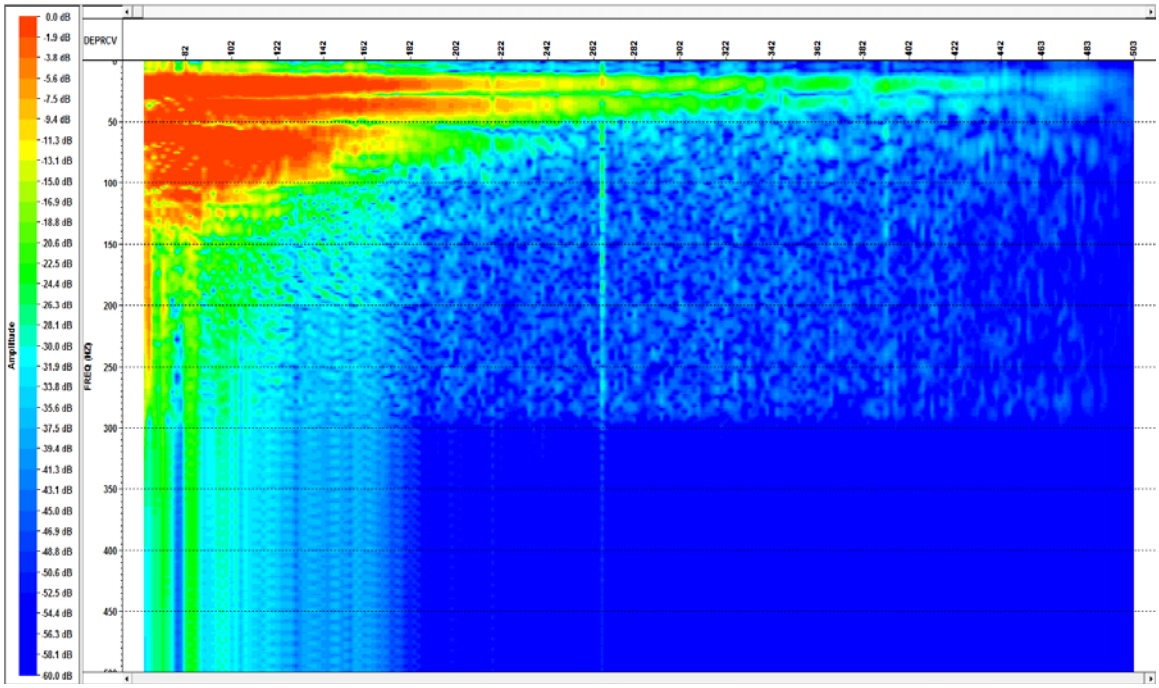

FIG. 26. Amplitude spectra of the down-going wavefield (shear waves). Notice that the loss of amplitudes with depth accurs more quickly than for p-waves.

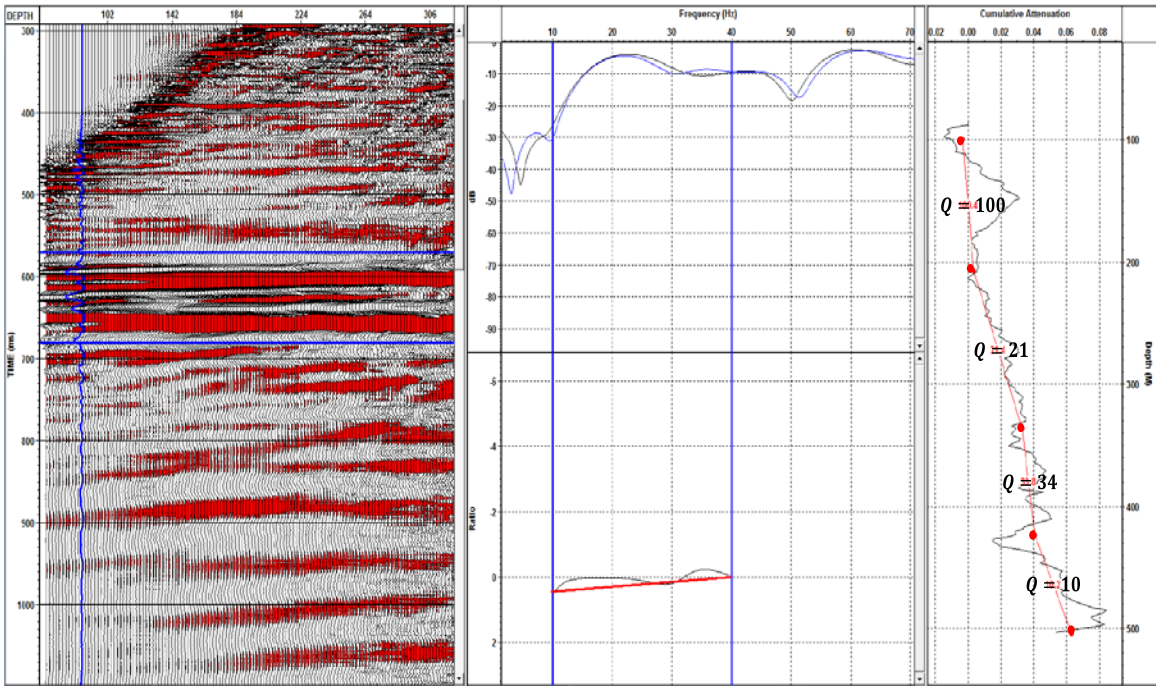

FIG. 27. Q_S estimation from down-going wavefield using spectral-ratio method (Vista software).

Q_P estimation using dominant frequency method (CREWES toolbox)

Field VSP data was also processed in Matlab, with Q_P values being estimated using the dominant frequency method in the CREWES toolbox. The traces were compared every 100 m to estimate Q_P from the down-going wavefield for both dynamite and EnviroVibe (red line, Figures 28 and 29). Q_P estimation from the up-going wavefield was only computed with the dynamite source (green line, Figure 28) and a distance of 150 m was used to compare the traces. The results obtained are shown in figure 30. As we observe, Q_P values estimated from the down-going wavefield are approximately 100 from 100-250 m depth and around 50 from 250-450 m depth. Those depths in which *Q=0* or *Q=250*, we could not obtain an accurate estimation, because of the noise in the data. Q_P values estimated from the up-going wavefield are approximately 40 from 100-250 m depth, which is lower than the estimated from the down-going wavefield. From the 250-450 m depth, the estimated Q is around 50 which matches with the results obtained earlier using the spectral-ratio method.

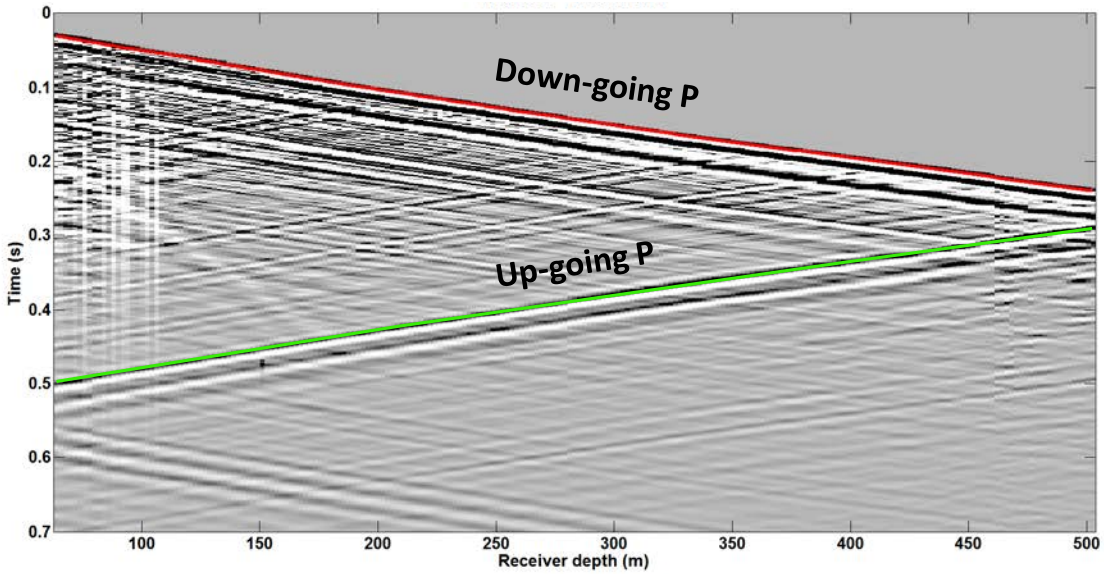

FIG. 28. Shot gather for shot point 1 with a dynamite source.

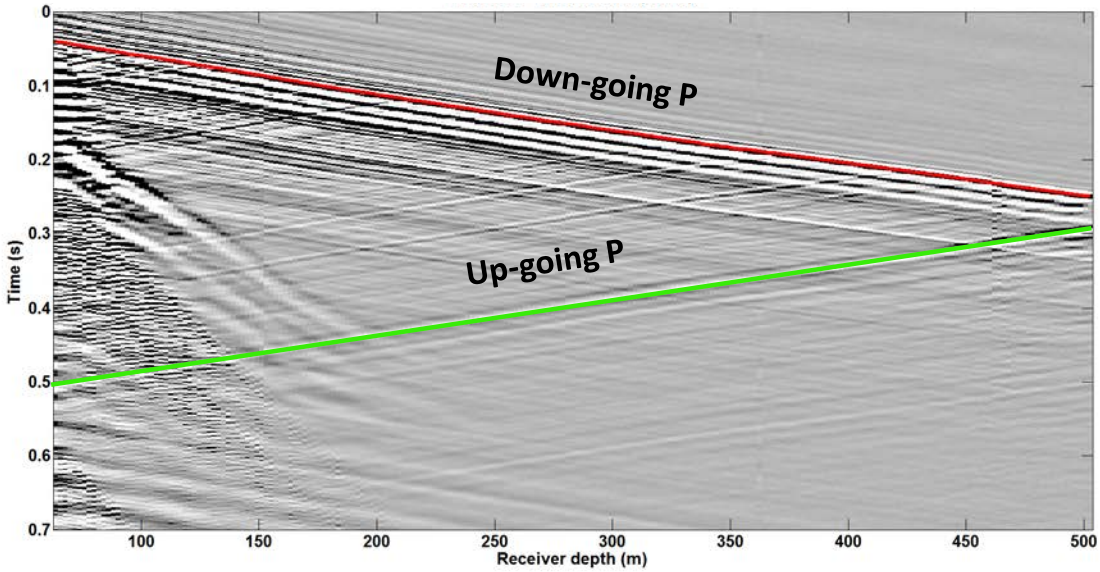

FIG. 29. Shot gather for shot point 1 with an EnviroVibe source.

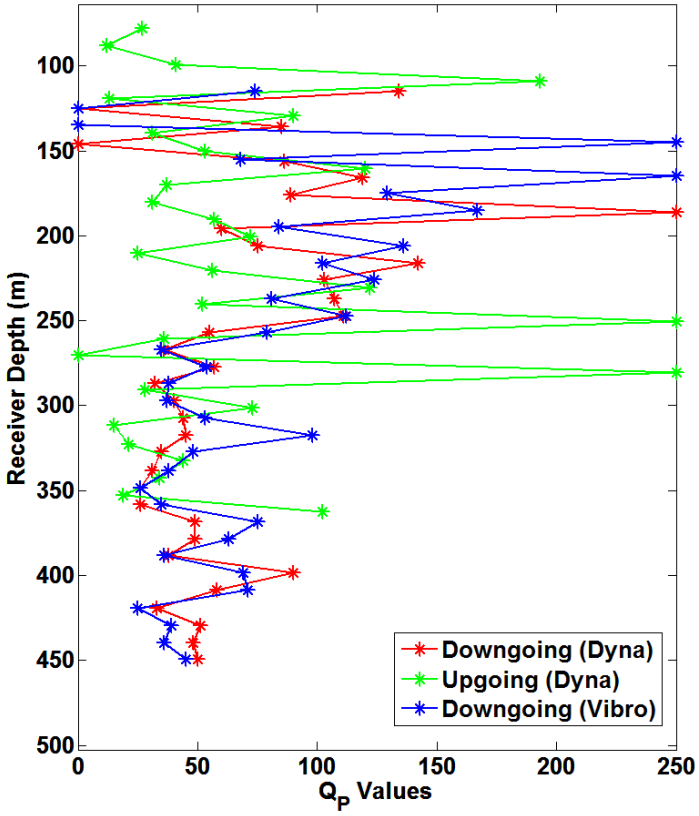

FIG. 30. Q_P estimations using dominant frequency method.

CONCLUSIONS

Q_P values were estimated from down-going and up-going synthetic VSP using the dominant frequency method. The best match between instantaneous Q and estimated Q was obtained comparing traces 50 m apart. Comparing traces that are too close together may lead to an estimate of Q values that are higher than the actual Q. On the other hand, if we compare traces that are too widely separated, we may obtain errors in our Q estimation because there is a higher risk that we compare traces from different layers.

Q_P estimation from the real VSP data was obtained using the spectral-ratio method from Vista software. When we chose a frequency window from 30-130 Hz to estimate Q_P from the down-going wavefield, we obtained similar results for both dynamite and EnviroVibe source. But if we expand the frequency window from 30-250 Hz, the results for the EnviroVibe data are lower. That is probably because the spectral-ratio method is more sensitive to the frequency band that we choose and also to the noise in our data. Q_P values were also estimated from the up-going wavefield where the main difference with the down-going wavefield is the result obtained in the shallow layer. There, the estimated Q_P value is lower since the wavefield has propagated a longer period of time at that zone. Then, it will observe more significant attenuation when we process the data. The spectral-ratio method was also used to estimate Q_S values from the real down-going wavefield for EnviroVibe source. Results show that Q_S values are lower than Q_P.

Q_P estimation from real VSP data was also computed using the dominant frequency method from CREWES toolbox. The results obtained from the down-going wavefield are similar for both dynamite and EnviroVibe source. Q_P values estimated from the up-going wavefield matches with the down-going wavefield for overall, but for the shallow layer the Q values are lower than before.

FUTURE WORK

Ideas for future work include:

- Adding noise to the synthetic VSP to study how the noise affect our Q estimation.
- Performing an elastic forward modelling using shear wave velocity from well logs close to borehole. Then, compute a synthetic VSP to estimate Q_S values.
- Q_P and Q_S estimation from offset VSP data. The X component of the offset VSP shots shows an up-going shear wavefield with a strong energy that can be used to estimate Q_S.

ACKNOWLEDGEMENTS

We thank an unidentified company for access to the field VSP data. We thanks GEDCO/Schlumberger for providing the VISTA software. We thank sponsors of CREWES for their support. We also gratefully acknowledge support from NSERC (Natural Science and Engineering Research Council of Canada) through the grant CRDPJ 379744-08.

REFERENCES

Aki K., and Richards, P. G., 2002, Quantitative Seismology 2nd Edition, University Science Book.

Cheng, P., Margrave, G. F., Comparison of Q-estimation methods: an update: CREWES Research Report, 25, 14.1-14.38.

Hinds, R. C., Anderson, N. L., and Kuzmiski, R. D., 1996, VSP Interpretive Processing: Theory and Practice, Soc. Expl. Geophys.

Kjartansson, E., 1979, Constant Q-Wave Propagation and Attenuation, Journal of Geophysical Research, 84, 4737-4748.

Margrave, G. F., 2013, Q tools: Summary of CREWES software for Q modelling and analysis: CREWES Research Report, 25, 56.1-56.22.

Margrave, G. F, 2013, Method of Seismic Data Processing. Course Lecture Notes, Univ. of Calgary.

Margrave, G. F., 2014, Synthetic seismograms with Q and stratigraphic filtering: CREWES News, 26, Issue 2, p. 6-7.

Quan, Y., and Harris, J. M., 1997, Seismic attenuation tomography using the frequency shift method: Geophysics, 62, 895-905.

Hall, K. W., Lawton, D. C., Holloway, D., and Gallant, E. V., 2012, Walkaway 3C-VSP: CREWES Research Report, 24, 9.1-9.26.